

Topseal integrity assessment using seal properties and leakage phenomena

M. Foschi^{a,*}, P. Van Rensbergen^b

^a Department of Earth Sciences, University of Oxford, South Parks Road, Oxford, OX1 3AN, UK

^b Shell Global Solutions International BV, Kessler Park 1, Rijswijk, 2288GS, the Netherlands

ARTICLE INFO

Keywords:

Seal failure

Natural leakage

CCS

Seismic interpretation

Centroid analysis

ABSTRACT

We present a novel seismic interpretational workflow applied to a large gas-chimney located above the Marjoram Gas Field, offshore NW Borneo. The gas-chimney is hosted by a clay-dominated sealing sequence characterised by meter-scale silt beds. The sealing sequence is affected by a complex network of normal faults. The gas chimney, interpretable as vertical anomaly cluster, is composed of several discrete amplitude anomalies and is the result of gas leakage from the crest of a ~500 m thick carbonate pinnacle-reef below. By analysing the seal properties and the anomalies composing the vertical anomaly cluster we argue that the leakage is consistent with migration of gas either along faults or using faults via cross-fault-plane juxtapositions. We show that this process is focussed within a narrow pathway rather than spread over the fault network. Mode I fault opening in response to the large capillary pressure exerted by the long gas column of the subjacent Marjoram Gas Field is postulated to be the cause of leakage.

1. Introduction

Topseal leakage is an important risk in retaining subsurface fluids for example in hydrocarbon exploration (Mathieu, 2015; Myers et al., 2019; Rudolph and Goulding, 2017) and in several applications, such as subsurface storage of carbon dioxide (CO₂; Smith et al., 2013). Evidence of leakage is common, and it is frequently observed on seismic data (Andresen et al., 2011; Arts et al., 2004; Cartwright and Huuse, 2005; Foschi and Cartwright, 2016; Løseth et al., 2009). However, case studies using detailed analysis of the associated expressions of hydrocarbon anomalies to understand the leakage path and origin are relatively few (Foschi and Cartwright, 2020).

The most common seismic evidence of leakage from topseals is probably that of gas chimneys (Judd and Hovland, 1992; Heggland, 1997, 1998). Gas chimneys were known in the industry back in the 50's although well-known examples were published in the 80's in association with the discovery of large oil fields in the Central Graben of the Norwegian North Sea (e.g., Munns, 1985). Of the various early definitions of gas chimneys, we adopt in this study that proposed by Heggland (1997), who described gas chimneys as zones of seismic disturbance characterised by distortion of amplitudes and phase of the background reflectivity (Heggland, 1997). The interest in gas chimneys as evidence of leakage, combined with the strong deterioration of the seismic imaging that accompanies their geophysical detection, allowed several

theories to be postulated in the last 30 years. An incomplete and brief list of works addressing the significance of gas chimneys in chronological order is then presented below.

In 1998, Bjorkum (1998) theorized gas chimneys as a form of exsolution of gas escaping in solution from hydrocarbon fields. The mechanism invoked was related to the fact that water can move across capillary barriers (even at irreducible water saturations, Teige et al., 2005) and that a substantial proportion of gas can therefore move in-solution across the caprock and exsolve due to pressure drop above the seal. In the following year, Granli et al. (1999), in an early attempt to improve the imaging across gas chimneys, showed that the analysed gas cloud from the Tommeliten gas field was emplaced by migration of free phase gas leaking across the caprock, but via fault-related conduits.

A few years later Løseth (2002) postulated that gas chimneys above the Gullfaks South Field were formed by hydraulic fracturing of the seal and added, therefore, in the mechanism of their formation a condition of overpressure. The author reached this conclusion because of the high pore-fluid pressure and thermogenic gas concentration encountered within the drilled chimney with respect to nearby offset wells (Løseth, 2002). The combination of (i) high pressure, (ii) generation of fractures and (iii) formation of gas chimneys was then studied in the following years. Arntsen et al. (2007), among others, modelled the gas chimney above the Tommeliten Alpha field as a fracture network filled with gas. The imaging resulting from the seismic forward modelling was

* Corresponding author.

E-mail address: martinfofchi@earth.ox.ac.uk (M. Foschi).

<https://doi.org/10.1016/j.marpetgeo.2022.105573>

Received 27 September 2021; Received in revised form 21 December 2021; Accepted 1 February 2022

Available online 10 February 2022

0264-8172/© 2022 The Authors. Published by Elsevier Ltd. This is an open access article under the CC BY license (<http://creativecommons.org/licenses/by/4.0/>).

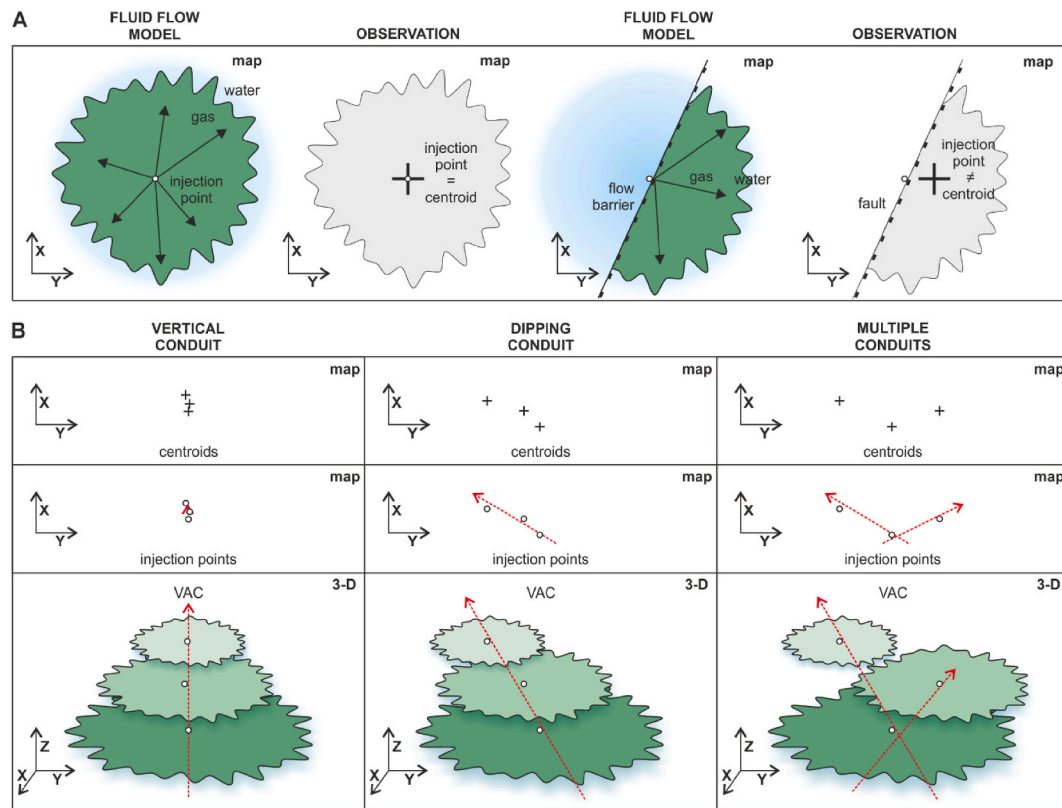


Fig. 1. A, simplified cartoon showing the spreading of gas from an injection point in water-saturated homogenous horizontal media. The gas generates a circular region by displacing water radially down a radial pressure gradient (e.g., Zhao et al., 2016). However, if flow barriers are present, a perfectly circular gas region may not form, and the position of the centroid will not represent the injection point. B, simplified cartoons showing the distribution of centroids and injection points in map view, and 3-D expression of VACs formed by a single vertical (left) and plunging (center) conduits, and multiple conduits (right). Centroid distribution associated with vertical conduits have been observed in block A and B, offshore Dutch (c.f. Foschi et al., 2018). Plunging conduits are observed in this study. Red arrows indicate the indicative direction of flow across the intervening stacked reservoirs. (For interpretation of the references to colour in this figure legend, the reader is referred to the Web version of this article.)

comparable with the seismic response from the real analogue.

Heggland (2005, 2013) then recognised that the position and the geometry of gas chimneys could reflect the location of seal failure and that using these observations the interpreter could increase the rate of discoveries. Bello et al. (2017) extended Heggland's (2005) work in trying to address the presence of high pressure within gas chimneys. The authors concluded that, within a population of about 80 examples, only a subset of the analysed gas chimneys was indeed associated with a condition of overpressure. That study demonstrated that overpressure might not be related to gas chimneys but could not address whether a condition of overpressure was present before, or during, leakage.

Back with the same line of research of Arntsen et al. (2007), Rubino et al. (2011) presented a geological model composed of patchy distribution of CO₂ in stacked layers but without a fracture network. The seismic output resulting from the forward modelling was very similar to previously reported gas cloud observed on seismic data (e.g., Arts et al., 2004). On the same line of research of Granli et al. (1999), instead, Warner et al. (2013) demonstrated that the gas chimney above the Tommeliten Alpha structure (same example as in Arntsen et al., 2007) was consistent with poorly resolved layers charged with gas. The results, based on anisotropic full-waveform inversion techniques, were in line with the models proposed by Rubino et al. (2011), indicating stacked gas-charged reservoir and no fractures.

Later, Foschi et al. (2014) reinterpreted about 50 gas chimneys from the Falkland Plateau Basin, as stacked gas-related amplitude anomalies, and called these features vertical anomaly clusters (VACs). The interpretational framework, consistent with the works of Rubino et al. (2011) and Warner et al. (2013) allowed a more systematic analysis of these

leakage phenomena. Moreover, the interpretational approach raised the potential to define the migration mechanism based on the distribution and characteristics of the anomalies composing VACs (Foschi et al., 2014). Foschi et al. (2018) applied the VAC-related type of analysis to stacked gas reservoirs belonging to gas chimneys from offshore Netherlands (Blocks A and B). The cross-stratal migration responsible for the formation of the documented VACs, reconstructed using the centroids of the constituent stacked anomalies, was demonstrated to occur in a specific region within the common centre of the VACs. In Foschi et al. (2018) an overpressure of the gas phase (capillary pressure) was assumed to be necessary to overcome the capillary entry pressure of the seals in between the reservoirs but not necessarily as such to fracture the overburden (Foschi et al., 2018).

In this study, we analyse a large gas chimney above the Marjoram Gas Field, offshore NW Borneo (Fig. 2, inset). We apply and test the same interpretational framework as used for the analysis of stacked gas reservoirs documented by Foschi et al. (2018). We analyse the geometry of leakage in relation to overburden and seal characteristics and where the gas provenance is demonstrably linked to the reservoir underneath. We interpret the gas chimney as a structure characterised by an organised distribution of gas in layers (c.f. Rubino et al., 2012; Warner et al., 2013) and consistent with VAC's type mode of gas migration (Bertoni et al., 2018; Foschi et al., 2014, 2018).

The aim of this study is to demonstrate a rigorous method of defining the dominant leakage pathway and mechanism above the Marjoram Gas Field. The methods applied in this work, based on centroid and other analyses (c.f. Foschi et al., 2018), show that gas migrates vertically along faults but that the across-strata migration demonstrably focusses into a

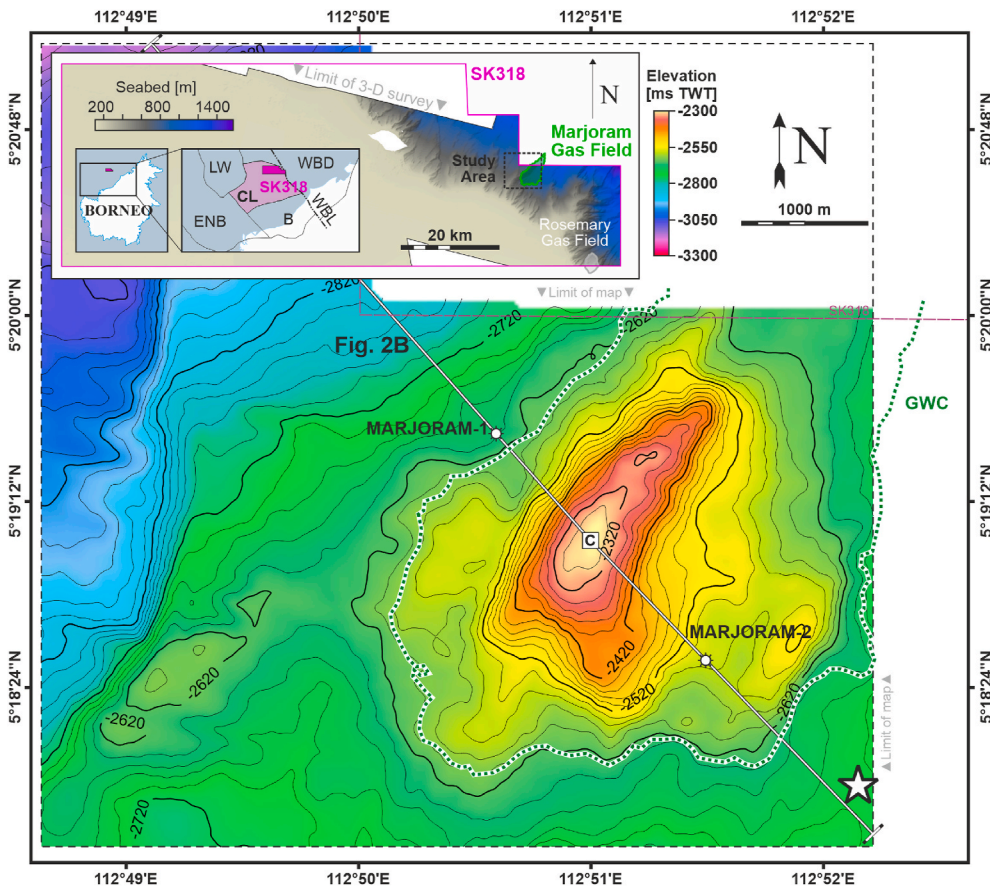


Fig. 2. Depth-to-two-way-time converted structure map of the “Top of Carbonate” (ToC) with location of crest (C), wells Marjoram-1 and Marjoram-2, spill-point (star, SE corner of the map), extent of the gas water contact (GWC), inset with location map and position of the cross-section shown in Fig. 3B. The location map shows the position of the license block SK318, the 3-D seismic volume and the position of the Marjoram and Rosemary gas fields. The block SK318 is located to the NW of Borneo and within the Central Luconia (CL) province. The study area is located towards the NE of the 3D survey where a prominent shelf break reflects the structural change from the Central Luconia to the West Baram Delta (WBD) structural provinces. The ToC map shows the prominent crest located to the southern portion of the GWC. The map is characterised by an uncertainty of ± 70 –80 ms TWT (~ 60 m). B = Balingian province; LW = West Luconia; ENB = East Natuna Basin; WBL = West Baram Line.

narrow central corridor of a fault array that also intersects the reservoir of the Marjoram Gas Field beneath. The workflow used in this study can be integrated into seal assessment workflows applied to oil and gas fields, but also to subsurface storage of CO₂.

1.1. Conceptual background to centroid analysis

As experimentally demonstrated, the injection and spreading of a non-miscible fluid into a fully saturated homogenous horizontal media (e.g., methane or CO₂ in water-wet reservoir) produces a sub-circular region (e.g., Zhao et al., 2016) whose centroid, the arithmetic mean of the point-coordinates of that region, approximately matches with the location of the injection point (Foschi et al., 2018). Similarly, the centroid of a sub-circular gas accumulation, interpreted for instance on seismic data, under specific circumstances, can provide the location of the injection of gas into the observed host formation (Foschi et al., 2018) (Fig. 1A). If the fluid conforms to structure (stratigraphic or fault trap) or the fluid is injected within a dipping reservoir (e.g., Luo et al., 2011), or the injection of gas occurs next to, or at, an impermeable barrier, such as a sealing fault, the centroid, resulting by the geometry of the gas accumulation, do not match the injection points (Fig. 1A).

When the migration process occurs across multiple reservoirs, such as in VACs, the positions of the centroids of the constituent gas accumulations provide the position, and the geometry, of the three-dimensional (3-D) migration pathway (Foschi et al., 2018) (Fig. 1B). The pathway can be related to a region of focussed migration across the porous media (capillary invasion), expressed as vertical distribution of centroids, or to a dipping conduit, such as a fault, where centroids are distributed following the dip of the conduit. Multiple trends of centroids highlights multiple conduits (Fig. 1B).

2. Data and methods

The database used in this study is a combination of 3-D dual-azimuth broadband seismic data and well data. The seismic data were acquired by Sarawak Shell Berhad in 2012 and cover an area of 3100 km² (Fig. 2, inset). The data volume is characterised by a bin size of 25 m and a sampling interval of 4 ms. The data was processed using a sequence suitable for preserving low frequencies and was finalised using American polarity – an increase of acoustic impedance contrast is characterised by a positive reflection coefficient (RC + Peak). The dominant frequency is 40–45 Hz (within the first 2 s TWT below the seabed) and yields a seismic resolution of ~ 10 m (c.f. Widess, 1973).

The well data comprises logs measured after the drilling of the two boreholes Marjoram-1 and Marjoram-2 (Fig. 2). The well data include gamma-ray, resistivity, sonic, and density logs, among others. The well database includes also well reports, inclusive of cuttings and lithological description of the encountered formations, fluid samples analysis, pressure data (pressure tests), and leak-off tests (LOTs). Shell International BV made these reports and other supporting information available, including depth-to-time converted surfaces of the main stratigraphic horizons and cultural data (e.g., coastline, license blocks and field outlines).

The methods used in this work comprise standard reflection seismic interpretation and amplitude extraction, on both amplitude and variance attribute, using Schlumberger’s Petrel software, and geometrical analysis tools. These tools, including the centroid analysis (c.f. Foschi et al., 2018), have been developed in Mathworks’s Matlab. A simple time-to-depth conversion of key horizons was performed using a one-dimensional (1-D) interval velocity function consisting of two layers, water (1500 m/s) and overburden (1600 m/s). The latter was estimated from well logs and check-shot tables.

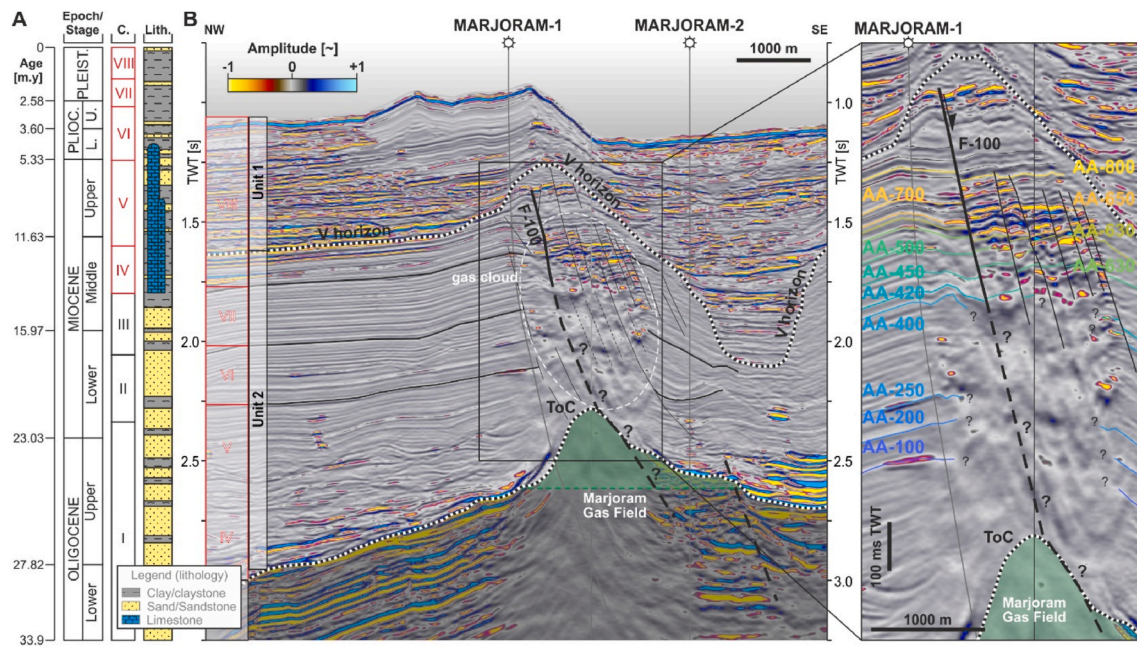


Fig. 3. Representative stratigraphic column of Central Luconia with subdivision into Cycles (C.) and Lithology (Lith.) (A; mod. from Lau et al., 2014), and 2-D cross-section across the crest of the Marjoram gas field and intersection with boreholes Marjoram-1 and Marjoram-2 (B; see Fig. 2 for line location). The cross section has a vertical exaggeration of about 2.7x. The study interval encompasses the upper cycles of the stratigraphic column from Cycle IV to Cycle VII. Prominent reservoirs are represented by the carbonate pinnacles developed from the Middle Miocene onwards. The source rock was encountered below the adjacent Rosemari Field (see Fig. 2 inset). The sealing unit encompass mainly the upper clay/claystone dominated cycles IV to VI and embeds several thief sands. The cross-section clearly depicts the Marjoram Gas Field structure and the large gas cloud/chimney characterised by amplification and distortion of the background reflectivity. The overburden is transacted by a SE dipping fault network. A major fault, fault F-100, transects the entire overburden from the ToC to the top of the gas cloud. The interpretation of fault F-100 is uncertain within the gas cloud (?). Several amplitude anomalies have been extracted along the gas cloud and used as input for the geometrical analyses (close-up; see text).

3. The central Luconia province

The Central Luconia province is bounded to the East by the West Baram Delta and to the West by the West Luconia and the East Natuna basins. A structural lineament known as the West Baram Line bounds the eastern margin of Central Luconia and separates the province from the West Baram Delta (Fig. 2, inset; Doust, 1981). Bathymetrically, the Central Luconia province exhibits a flat seabed surface dipping gently to NE and characterised by a water depth of about 200 m. In the north-eastern portion of the Central Luconia, a NW-SE oriented slope reflects the structural change from the Central Luconia to the adjacent West Baram Delta (Epting, 1980). The study area and the Marjoram Gas Field are located along this structural lineament (Fig. 2, inset).

The Cenozoic sedimentary column of the Central Luconia is characterized by a total thickness of about 2500 m (Fig. 3A). The sedimentary package towards the North of the province is divided into 8 cycles (I to VIII) with age ranging from Eocene to the Present. Each cycle is regressive and is separated by transgressive stages (Koša, 2015). The occurrence of carbonate features, such as carbonate build-ups and platforms, is observed throughout the sedimentary package, however during the Middle to Late Miocene (Cycle IV-V) the basin experienced a major period of carbonate deposition (Epting, 1980). Carbonate pinnacles and mega platforms developed mostly in the central and northernmost portions of Central Luconia with thick edifices spanning the entire sedimentary column (>2000 m). The carbonate build-ups are characterised by transgressive to high-stand carbonate facies. The margins of the major platforms and pinnacles are generally composed of high-energy formations, such as coral framestone. The internal facies are instead generally more mud-dominated limestone (Lau et al., 2014; Mehta et al., 2016). Carbonate build-ups in the southern portion of Central Luconia are more influenced by siliciclastic input (Rankey et al., 2019).

The Central Luconia province does not show evidence of tectonic activity after Middle Miocene (Epting, 1980). This condition is reflected by the absence of recent structures in the province and by a negligible anisotropy of the stress field (King et al., 2010). Nevertheless, minor normal faults, related to differential compaction, are often observed along the margins of the carbonate platforms. These affect the immediate formations above the carbonate build-ups and the overburden (see later).

The Central Luconia province is a very prolific area with over 65 trillion cubic feet (TCF) of thermogenic gas discovered to date (Janjuhah et al., 2018). The petroleum system is sourced from high-maturity Late Oligocene/Early Miocene Cycle I coals and terrestrial organic matter (Fig. 3A) (Lau et al., 2014; Mehta et al., 2016). The main reservoir targets are represented by over 200 carbonate build-ups (Epting, 1980). The sealing unit is represented by an Upper Miocene – Pliocene shale-rich package (Cycles IV to VI) (Fig. 3A) (Lau et al., 2014; Mehta et al., 2016).

The seal unit includes thief-sand intervals mainly within the upper Cycle V (Lunt and Madon, 2017). The Marjoram Gas Field, which represents the focus of this study, is a 2.4 TCF gas field (P50; gas initially in place) located to the NE of Central Luconia (Fig. 2 inset). The two wells Marjoram-1 and Marjoram-2 were drilled in 2014 and 2016 respectively, and gas composition is consistent with a wet-gas mixture.

4. Geological and geophysical observations

4.1. Reservoir

The Marjoram reservoir consist of a Post-Mid Miocene (Cycle IV) reefal carbonate (Lau et al., 2014; Mehta et al., 2016). The lithology of the reservoir is consistent with clean limestone with just a 20 m bed of muddy limestone (marl) towards the top of the interval (Fig. 4). Analysis

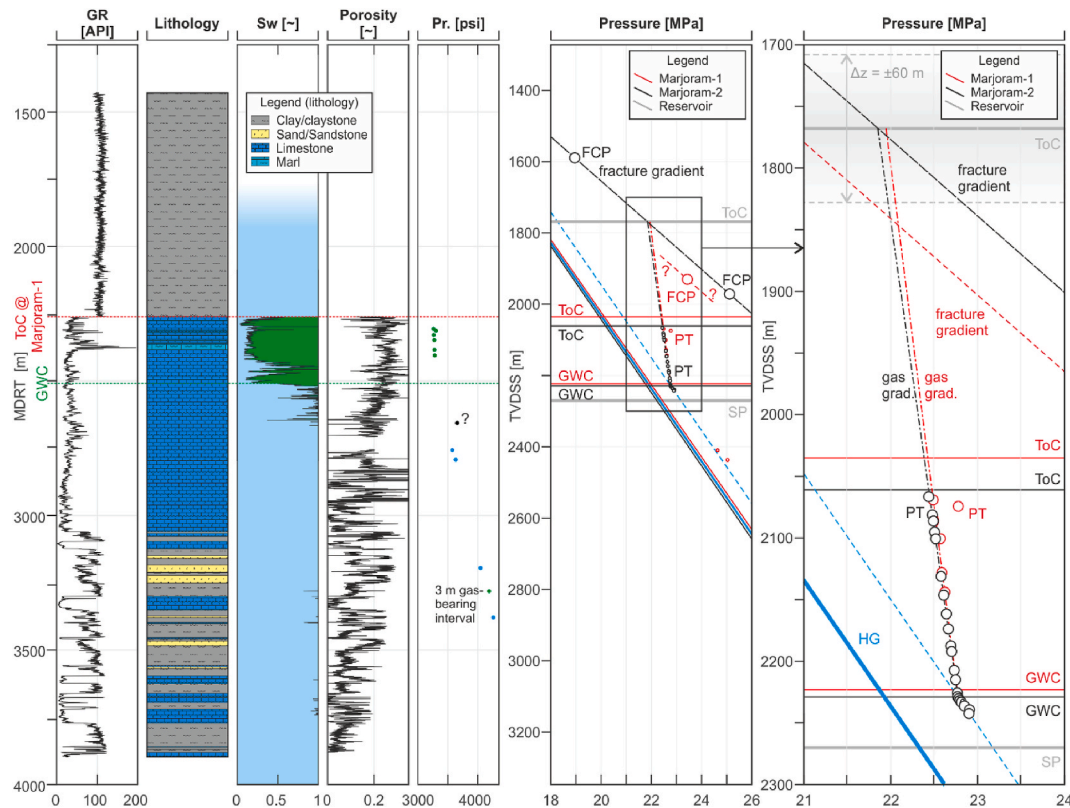


Fig. 4. Selected wireline logs from borehole Marjoram-1 (left) and pressure depth plot reconstructed using pressure tests performed at both Marjoram-1 and Marjoram-2 (right). The gamma-ray (GR) response along Marjoram-1 shows a clear decrease at the intersection between the seal and the Top of Carbonate (ToC). Lithological information retrieved using cuttings (Lithology) shows the excellent continuity of the reservoir above and below the gas water contact (GWC). The gas saturation within the reservoir interval is around 0.82 (S_w = saturation in water). The GWC can be identified by the intersection of the gas and water gradients reconstructed using the pressure tests (PTs). The compilation PTs and fracture closing pressure data (FCP) from both wells allowed to reconstruct the pressure setting within the reservoir, and the strength of the seal. An overpressure of ~ 0.8 MPa can be observed by comparing the water gradient derived from both wells using PTs (blue dashed line) and the hydrostatic gradient (HG) calculated using the water density from samples within the water leg of both Marjoram-1 and Marjoram-2. The projection of the gas gradients to the absolute crest of the reservoir coincides exactly with the measured fracture closing pressure (see close-up; ToC). The ToC surface bears an uncertainty of ± 60 m. MDRT = measured depth relative to the Rotary Table; SP = spill point; TVDSS = true vertical depth relative to the sea surface. (For interpretation of the references to colour in this figure legend, the reader is referred to the Web version of this article.)

of log data confirms a porosity range for the ‘cleaner’ carbonate facies of 0.20–0.25 and importantly no barriers/baffles are present within the carbonate reservoir section (i.e., net-to-gross = 1). The hydrocarbon saturation is about 0.82 (water saturation, $S_w = 0.18$) (Fig. 4).

Pressure data collected during the drilling of Marjoram-1 (Fig. 4) and Marjoram-2 is consistent with continuous gas columns of 188 m and 167 m, respectively. The total column from the GWC to the crest of the pinnacle is 455 m. Formation pressure testing revealed that the reservoir is ~ 0.8 MPa above hydrostatic. The geofluids within the reservoir section exhibit a “wet” composition dominated by methane and other light hydrocarbon phases (methane 55% by weight).

4.2. Seal and overburden

The overburden, the sedimentary interval from the ToC to the seabed, constitutes the sealing formation of the Marjoram Gas Field. The overburden encompasses the entire sedimentary column from Cycles IV to VIII (Fig. 3A) with a total thickness of about 1130 ms TWT, or about 900 m (using an interval velocity of 1600 m/s; Fig. 3). Above the Marjoram Gas Field, the overburden exhibits two contrasting seismic facies here called Units 1 and 2 (Fig. 3B).

Unit 1 extends from the seabed to a “V” shaped erosional surface, called here “V horizon”, located at about 370 ms TWT below seabed (or 300 m; Fig. 3B). Unit 1 exhibits seismic facies dominated by bright undulating reflections characterised by anomalies of both positive and negative response (Fig. 3B). The seismic facies is consistent with

vertically stacked 20–50 m thick mass-transport deposits, and oriented perpendicular to the shelf break (direction of sediment flow): approximately NE. Unit 2, based on cuttings from Marjoram-2, is composed of interbedded shale, silt and minor sand lenses, the latter occasionally overpressured.

Unit 2 extends from the V Horizon to the ToC (Fig. 3B). The average thickness above the Marjoram gas Field is in the order of 600 m. Seismically, Unit 2 is predominantly composed by parallel reflections characterised by low to moderate amplitude response (Fig. 3B). This second unit, based on cuttings from Marjoram-1, is composed of shaly claystone with interbedded minor thin siltstone layers. Gamma-ray logs show relatively high readings with values in the order of 100 API (Fig. 3B) and minor heterogeneities.

4.2.1. Structural features

A network of normal faults transects Unit 2 from the immediate top reservoir to the top of Unit 2 (Figs. 3B and 5). The faults in the network dip to SE at about 50–60° (Fig. 3B). The fault system is poorly resolved within the gas cloud, so a tentative reconstruction of the faults above the crest of the reservoir was carried out by mapping discontinuities observed on amplitude maps (Fig. 5A, inset). Variance attribute was also used to highlight continuity of the individual horizons and fault segments. The result of this analysis, shown on two representative surfaces at the middle and the base of the gas cloud (Fig. 5B and C, respectively), shows that the faults in the network are characterized by lengths in the order of a few kilometres and spacing of a few hundred meters (Fig. 5A).

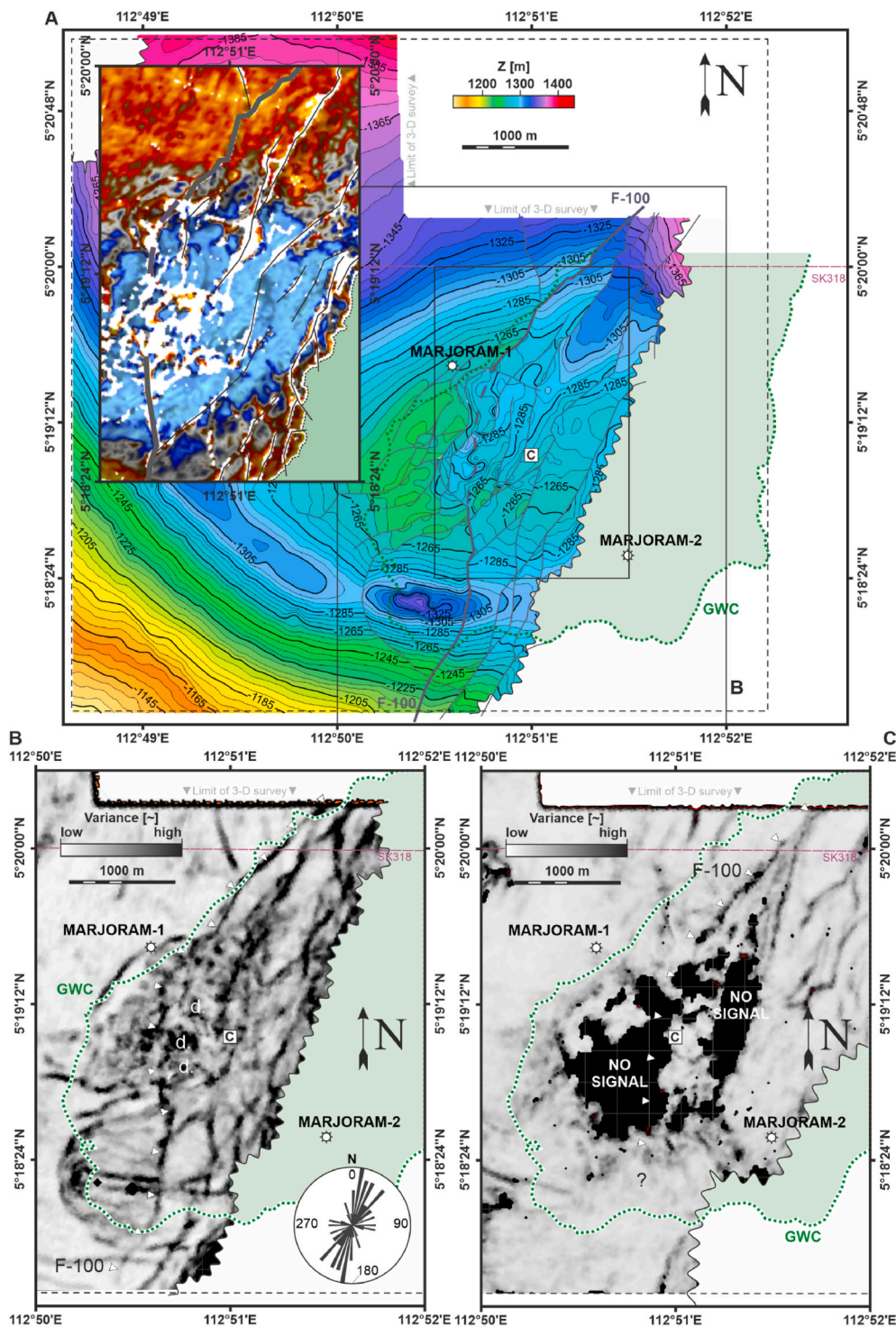


Fig. 5. Depth structural map from tentative interpretation of horizon AA-600 in the overburden (550 m above the ToC) with interpretation of the fault network, fault F-100, geographic position of the crest of the reservoir (C), geographic position of the gas water contact (GWC), location of the boreholes Marjoram-1 and Marjoram-2, inset showing the amplitude extraction with interpreted fault segments, and location of variance map in B and C. The depth reconstruction of this surface does not account for velocity variations caused by the gas cloud. The amplitude cut-offs of stratal bound anomalies (inset) have been used to reconstruct the NNE-SSW fault system and fault segment in A. Variance attribute extracted along horizon AA-600 (see Fig. 3B for horizon depth) with rose diagram of the fault orientation (B), and horizon AA-200 (see Fig. 3B for horizon depth) (C). The variance maps show continuous (B) and partially illuminate segments (C) of fault F-100 (white triangles). The variance attribute is sensitive to gas, resulting in distortion of the continuity of the fault segments (d., B). Faults, discontinuities, and reflectivity in general, are almost completely attenuated towards the base of the gas cloud (no signal, C).

The fault network is oriented mainly N–S and runs parallel to the eastern flank of the carbonate pinnacle hosting the Marjoram Gas Field (Fig. 5B, rose diagram).

A major fault, named here “F-100”, transects the overburden and the reservoir along the eastern portion of the carbonate build-up hosting the Marjoram Gas field, from North to South. Fault F-100 is continuous at the shallow section (Fig. 5B) although clear gas-related distortions are visible within the core of the gas cloud (Fig. 5B, “d.”). The fault, and the reflectivity in general, at depth, are obscured by the prominent gas cloud (Fig. 5C). The lack of imaging and signal deterioration preclude us to assess whether the fault is a continuous feature or composed of linked

segments.

F-100, and the main NNE-SSW fault system, are currently inactive as all the encountered fault tips terminate at the top of Unit 2 (Fig. 3B).

4.2.2. Trap capacity and seal strength

The structural relief of the trap, from the spill-point to the top of the pinnacle is about 500 m. The Marjoram Gas Field is then underfilled by 40–50 m. The strength of the seal (overburden), evaluated using leak-off tests performed during the drilling of Marjoram-1 and Marjoram-2, is characterised by a fracture closing pressure (FCP) gradient of 16.4 kPa/m (Fig. 4, pressure plots). The FCP gradient was reconstructed using well

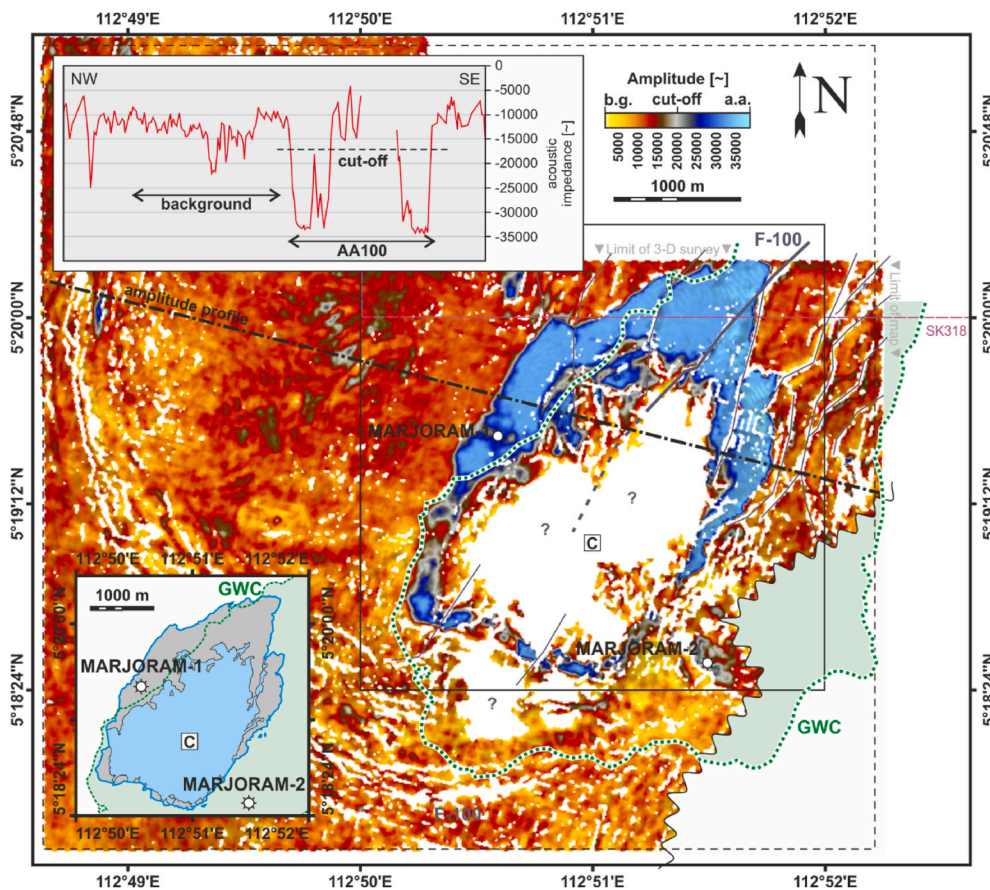


Fig. 6. Amplitude anomaly AA-100 with interpretation of the fault network, position of the crest of the reservoir (C), gas water contact (GWC), location of the boreholes Marjoram-1 and Marjoram-2, position of the amplitude profile shown in the inset, and the margin of AA-100 (inset). The anomaly is located along the westernmost portion of the GWC and slightly decentred with respect to the crest (C). The attenuation is prominent at the centre of the anomaly where a continuous interpretation was not possible (question marks). The amplitude extraction along the shown amplitude profile exhibits both background and amplified value. The cut-off selected for this anomaly, ~17000, provides the resulting margin in the inset at the bottom-left corner (grey area). The final margin used to extract the parameters of the individual anomalies is based on the light blue area (see text). (For interpretation of the references to colour in this figure legend, the reader is referred to the Web version of this article.)

formation test data retrieved within a window of 500 m above the ToC and so are representative of the portion of the intact seal hosting the gas cloud. The extrapolation of the gas gradients, retrieved from pressure and fluid density information from Marjoram-1 and Marjoram-2 (Fig. 4), reveals that at the crest of the carbonate pinnacle, located at 1768 m TVDSS, the pressure exerted by the gas column within the reservoir is approximately equal to FCP. The Marjoram Gas Field is at, or very close to, its top seal's FCP limit (Fig. 4), and is likely to be leaking hydrocarbons at present.

4.3. Vertical anomaly cluster

The gas chimney above the Marjoram Gas Field is clearly identifiable as a region of seismic amplification and distortion of reflectivity relative to the off-structure background (Fig. 3B, inset). This leakage feature has an irregular volume that crudely enclose a 3-D stack of elliptical shapes in map view and is entirely hosted within Unit 2 (Fig. 3B). The root of the gas chimney is at the crest of the carbonate pinnacle, which is in the SW of the gas field (GWC; Fig. 2). The gas chimney, interpretable as a vertical anomaly cluster (VAC, c.f. Foschi et al., 2014) has been divided into 10s of amplitude anomalies (see Data and Methods). The clearest interpretable anomalies, 12 in total, have each been individually included in this study and analysed.

4.3.1. Amplitude anomalies: acoustic description

The anomalies composing the VAC above the Marjoram Gas Field are soft in polarity and characterised by an acoustic amplification (in arbitrary amplitude units) around three times the background value (Fig. 6, inset). The amplification is interpreted to be related to the gas expelled by the underlying field and similar to the normal expression of amplifications attributable to free gas observed on seismic data (e.g., Sheriff, 1975). The amplification within the amplified zones is heterogeneous.

Nevertheless, a ceiling amplitude response is observed within the strongest amplified regions (see acoustic impedance around 33000 in Fig. 6 inset). This lack of variation of amplitude in the high value range is interpreted to be caused by the lack of sensitivity of the seismic reflection response to variations of gas saturation (c.f. Domenico, 1974).

Most of the anomalies observed within the VACs are characterised by a sharp decrease of amplitude at their centres (Fig. 6, question marks). This characteristic is interpreted to be caused by transmission artefacts (c.f. Sheriff, 1975) deriving from the ray paths through the shallower amplitude anomalies composing the VAC (Fig. 2B) and described in gas chimneys elsewhere (e.g., Arts et al., 2004; Arntsen et al., 2007; Foschi et al., 2018). The decrease of amplitude at the centre of the AAs is prominent at the basal anomalies, such as AA-100, where a continuous interpretation across the centre of the VAC is not possible (Fig. 6). Nevertheless, the free-gas regions responsible for the resulting anomalies are interpreted to be continuous across the attenuated regions (Fig. 6, insets, blue area/contour).

4.3.2. Amplitude anomalies: geometrical description

The geometrical description of the amplitude anomalies was based on the shape of their outer margins extracted at the interpreted amplitude cut-off (e.g., Fig. 6, insets). The amplitude cut-off was evaluated for each anomaly by defining background and amplified regimes. The exact threshold amplitude was calculated in the middle of the two defined average regimes. This method allowed to overcome the issue of local acoustic impedance ranges and local amplifications. The areas of the margins were further simplified and added to that of their respective central attenuated areas (Fig. 6, insets). These final combined margins and central area maps have then been used for geometrical and centroid analyses (Fig. 7).

The 12 anomalies exhibit an areal extent from 0.1 to 6.0 km² and are crudely elliptical in shape (their eccentricities measured using

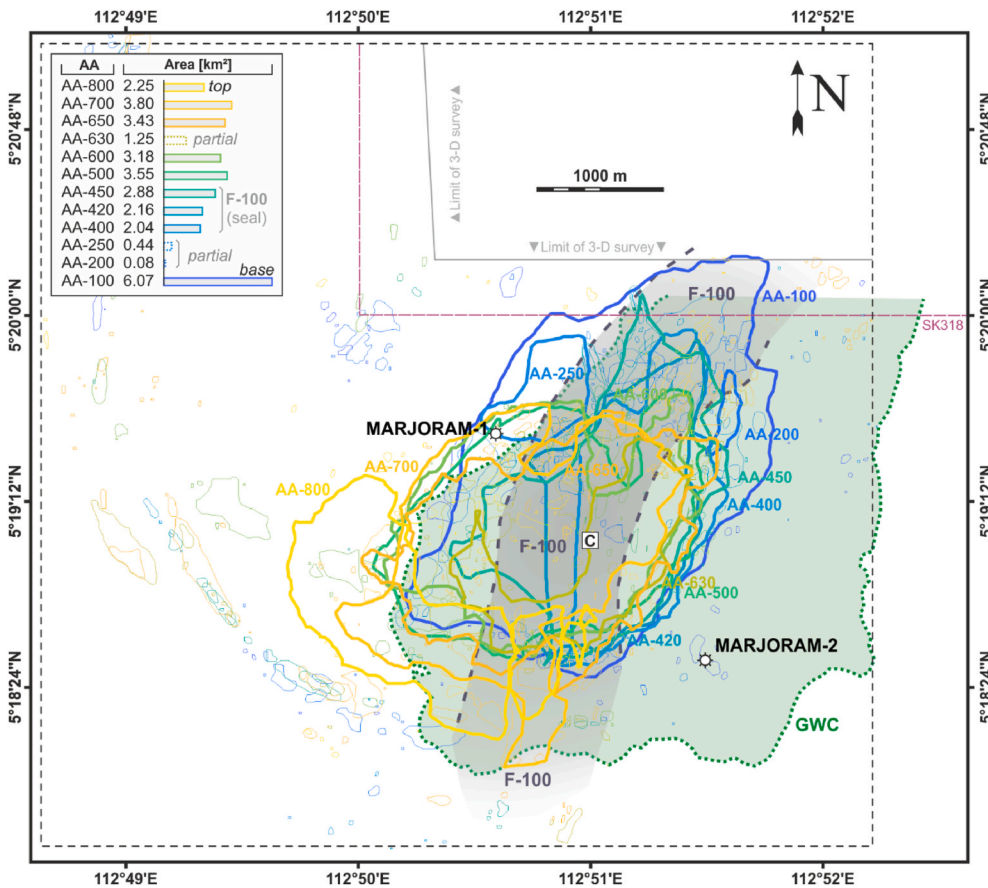


Fig. 7. Base map of the margins of 12 anomalies with tentative interpretation of fault F-100 from the Top of Carbonate to the top of the gas cloud, position of the crest of the reservoir (C), gas water contact (GWC), location of the boreholes Marjoram-1 and Marjoram-2 and inset with area of the name and area of the extracted margins. Only the largest anomaly for each interpreted horizon is labelled and highlighted with thick line. Partial interpretation at anomaly AA-200, AA-250 and AA-630 was due to attenuation and disruption (these anomalies will be discarded from the following discussion). The area of the anomalies includes attenuations and is assumed to be continuous across the entire anomaly extent. The area of the anomalies decreases non linearly from the base to the top of the VAC. Anomalies AA-400, AA-420 and AA-450 are bounded by fault F-100.

approximate axes lengths averages ~ 0.8). The area of the anomalies is affected by both structural elements (e.g., AA-420, shown later) and partial illumination (e.g., AA-250, Fig. 7, inset). These factors produce an unclear variation of area with depth. Nevertheless, the variation in area from anomaly AA-450 to AA-800 is small ($\text{std} = 0.55$). The distribution of the anomalies within the VAC is asymmetric. The anomalies located towards the top of the VAC are located to the SW with respect to the basal anomaly AA-100 (Fig. 7). Although this result will be explored more in detail with the centroid analysis it is worth noting here that the diagonally-offset distribution of the anomalies composing the VAC is different from previously reported analysis of stacked anomalies (Foschi et al., 2018), but also different from typical gas chimneys (Arntsen et al., 2007; Bello et al., 2017) and CCS related carbon dioxide clouds (e.g., Arts et al., 2004).

The juxtaposition of (1) the amplitude maps and calculated margins with (2) the depth contours of the relative time-to-depth converted host reflections (see Data and Methods), reveals that the anomalies do not precisely conform to structure. By looking at Fig. 8 (and accompanying Fig. 5A) AA-600 does not fill the shallower portion of the structure located at the footwall of F-100 and diverges with respect to the depth contour by about 20–25 m (Fig. 8, inset). The lack of conformity to structure could be related to lithological variation within the host units (small-scale stratigraphic trapping) or to a dynamic state of the gas in place or to velocity anomalies in the overburden. The application of a 1-D velocity model for conversion from time to depth could also be insufficient to resolve the exact geometry of the overburden and verify whether the anomalies conform to structure.

4.3.3. Amplitude anomalies and faults

The 12 anomalies are all transected by the NNE-SSW oriented normal faults that cut the overburden hosting the VAC (Figs. 3B and 5). The amplitude amplification of the anomalies is continuous across the fault

intersection towards the centre of the VAC (e.g., Figs. 6 and 8). This condition suggests that minor faults do not produce a flow barrier for the spreading of gas within the faulted host formations (discussed later). Far from the centre of the anomalies the margins are instead characterised by a sharper, planar offset pattern (e.g., Fig. 6). This evidence implies that fault displaces the hosting media but that the gas phase keeps hydraulic conductivity across the fault.

Conversely, larger faults, such as F-100, seem instead to affect the extent of a number of anomalies at the centre of the VAC by cross-fault sealing (see Fig. 7, inset). Specifically, F-100 bounds anomalies AA-400 to AA-450, in that they are present mainly within the hanging wall of this fault (e.g., AA-400, Fig. 9), and anomalies AA-500 and AA-540 whose shapes are shifted sinistrally with respect to the portion of the anomalies belonging to the footwall block (e.g., AA-500, Fig. 10). This evidence suggests that F-100 acts partially as barrier for lateral gas flow and affects the morphology of the VAC at its centre.

4.3.4. Centroid analysis

The centroids of the amplitude anomalies were calculated using the outline shapes (Foschi et al., 2018), i.e. the margins only and neglecting variations of amplitude, attenuations, and loss of signal within the anomalies (e.g., Fig. 6, blue contour). The position of the centroids was also evaluated in relation to structural features, such as faults. The centroid analysis is presented firstly with reference to two representative anomalies, AA-500 and AA-430, whose centroids are located at the centre of their simplified margins (Figs. 10 and 11).

Anomaly AA-500 (Fig. 10) exhibits attenuation and other transmission artefacts but is roughly subcircular in shape. Because of this shape we interpret that the spreading of gas was not influenced by structural barriers and that the centroid can be interpreted as the point, or region, subject to gas injection into the mapped horizon. For anomaly AA-500 the interpreted injection point is also placed a few 10s of meters

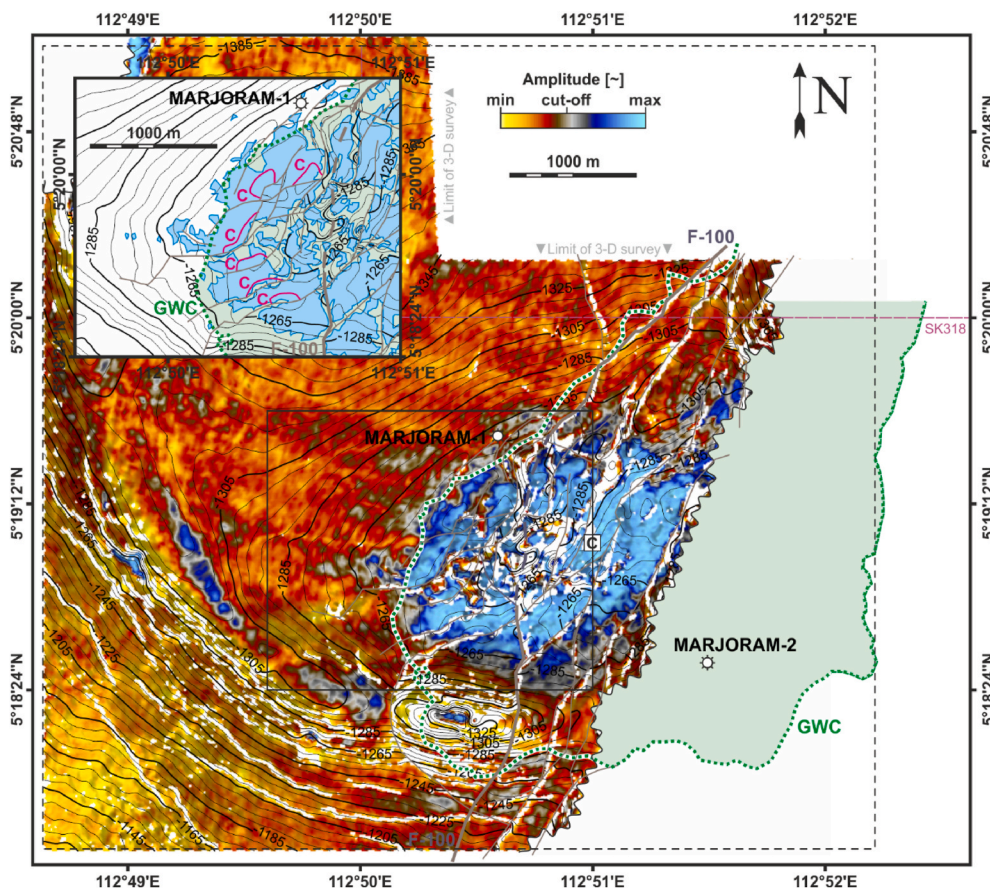


Fig. 8. Amplitude anomaly AA-600 with the depth contour at the same horizon, tentative interpretation of the fault network, position of the crest of the reservoir (C), gas water contact (GWC), location of the boreholes Marjoram-1 and Marjoram-2, and inset with its extracted margin. The anomaly is located towards the top of the VAC (see Fig. 7, inset) and is characterised by an elliptical shape. The margin of the anomaly crosscuts the depth contour at several points, and it is not centred at the crest of the structure, but offset to the SW (inset, c).

distant from the interpreted fault F-100 (Fig. 9). This close distance, between the interpreted injection point and the fault F-100, suggests that the latter might act as the region of gas injection into the host horizon.

Conversely, anomaly AA-450 (Fig. 11) is characterised by semi-circular shape indicating that gas was not able to spread in all directions. In this case the shape is affected by fault F-100 and the centroid is not interpreted as the injection point. For anomaly AA-450 the locus of gas injection could be placed anywhere between the actual centroid and fault F-100. Because AA-450 is part of a stack of anomalies the position of the injection point will be evaluated later once all other centroids are presented (see Discussion).

We then extend the centroid analysis and interpretation to all 12 anomalies and integrated the centroid distribution against the position of the crest of the reservoir, the fault network (interpreted towards the top of the VAC), and the GWC of the Marjoram Gas Field. The centroids of 3 anomalies, namely AA-200, AA-250 and AA-630, presented in the results, were discounted from the analysis and discussion because of their interpretation was only partial (Fig. 7, inset).

The result of the centroid analysis for the entire stack of anomalies (Fig. 12) shows that 12 centroids are in an area around, and to the East, of the crest of the reservoir (C, Fig. 12). The centroids follow a NE-SW oriented trend with an R^2 of ~ 0.4 . By removing the centroids of the partially interpreted anomalies (Fig. 7, inset) the R^2 increases to 0.8 (55°N). The centroids are clearly spread along a ~ 1.8 km long corridor characterised by a trapezoidal geometry on map view. Importantly, the depth of the centroids decreases systematically from NE, at the base of the VAC (AA-100), to SW, at the top of the VAC (AA-800). This specific

geometry defines then a clear inclined track from the base to the top of the VAC and rising to the SW. This pathway is interpreted to be the potential locus of the successive gas injection points for the formation of the VAC (see Discussion).

5. Discussion

5.1. Significance of the distribution of centroids

In Foschi et al. (2018) the (1) focused distribution of injection points within a narrow, vertical, columnar volume, (2) the relatively simple horizontal geometry of the host formations, and (3) the lack of structures, implied the presence of a vertical central region of focused fluid flow connecting several stacked reservoirs in vertical succession (vertical conduit, Fig. 1). The 9 selected injection points mapped above the Marjoram Gas Field are instead distributed along a plunging corridor (Fig. 11) whose root, here assumed to be the deepest centroid (belonging to AA-100), is located close to the crest of the reservoir and the location where F-100 intersects the ToC (Fig. 11). This specific distribution implies the presence of a preferential pathway which could be related to a fault, or several faults.

The presence of structural features within the overburden, in particular fault F-100 (e.g., Fig. 8) could have provided a preferential migration pathway for the formation of the VAC and is the simplest interpretation of the evidence. A more complex pathway whereby free gas flows via several pathways (c.f., Arntsen et al., 2007), not necessarily linked to fault F-100, could still take place. Nevertheless, the high R^2 resulting from the mapped injection points suggests that a single conduit

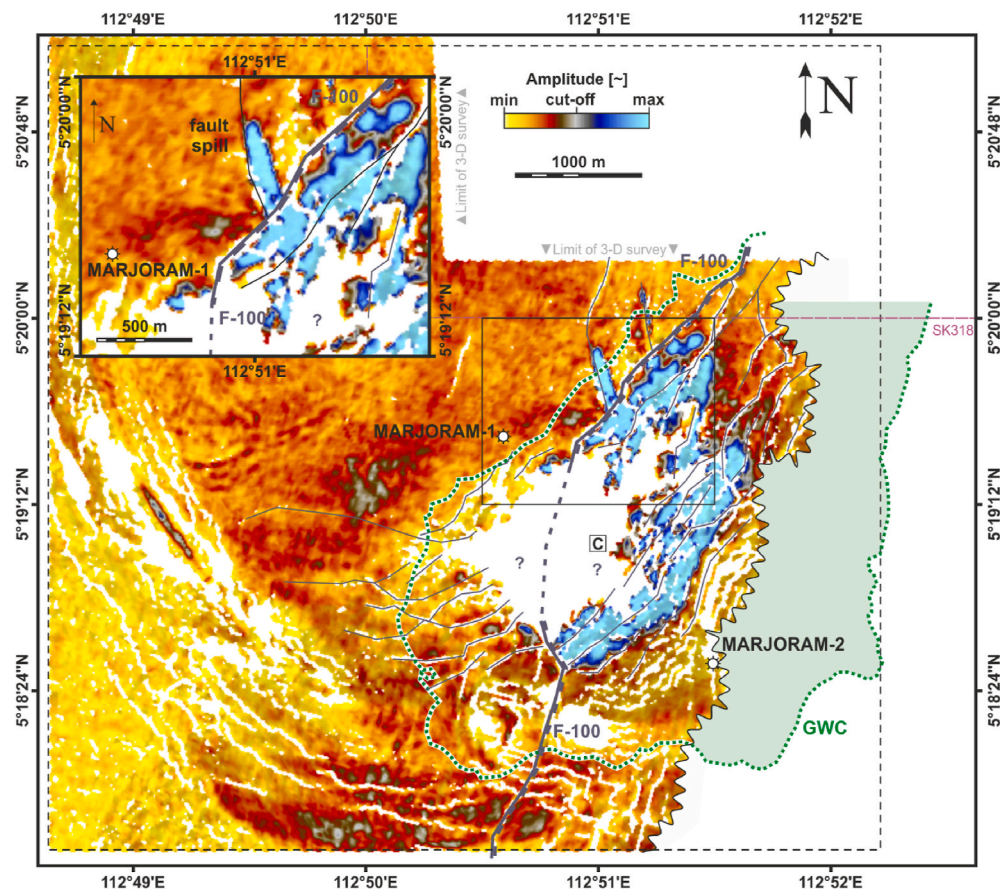


Fig. 9. Amplitude anomaly AA-400 with tentative interpretation of the fault network, position of the crest of the reservoir, location of the boreholes Marjoram-1 and Marjoram-2 with close-up (inset). The anomaly is not interpretable at the centre because of transmission artefacts (question marks). The western margin of the visible portion of the anomaly is bounded by fault F-100, however some gas migrated across the fault and into the footwall block (fault spill, inset).

is responsible for the migration of gas.

Based on the argument above, the injection points of anomalies AA-400, AA-420, and AA-450 could be relocated (Fig. 13A) or removed from the centroid analysis (Fig. 13B). The first option would see the centroids to move towards the intersection of the anomalies with fault F-100 (the most likely conduit). This relocation could be justified by the fact that some of the centroids are observed to be close to the fault F-100 intersection with the amplitude anomalies (e.g., A-500, Fig. 10). This manipulation of the centroids would increase R^2 to 0.88 (43°N) (Fig. 13A). The second option is instead to exclude the centroids from the centroid analysis. This operation is favored as a clear representation of fault F-100 is not possible within the disturbed region within the core of the VAC. The exclusion of the centroids of anomalies AA-400, AA-420, and AA-450 would increase R^2 to 0.94 (45°N) (Fig. 13B).

5.2. Migration pathway

The migration of hydrocarbons across the overburden needs to satisfy certain observations related to the VAC, such as the position of the injection points, the relationship between the anomalies and fault F-100, and other evidence related to the overburden including the structures and the pressure data. Because of poor imaging and lack of detailed knowledge of the permeability structure within and surrounding the conduit region (e.g., damage zone, number of fractures), the migration of gas through the overburden could be achieved either by (1) a combination of cross-stratal and horizontal migration stages (Fig. 13C), or

(2) exploiting fault F-100 and the damage zone related to it (Fig. 13D).

A “staircase” migration model requires as many stages of cross-stratal migration as stages of fluid flow along strata (Fig. 13C). For the vertical migration ones there must need a sort of conduit region for each step or a condition where the capillary pressure is larger than the capillary entry pressure of the intraformational seal (Berg, 1975). This scenario requires gas anomalies conforming to structure and a sequence of crestal culminations aligned exactly to the linear conduit reconstructed using the centroids. As observed on a representative map related to anomaly AA-650, the anomalies do not conform precisely to structure and the centroids are not placed at the indicated crestal culminations (Fig. 8, inset, c).

Moreover, within this model, the presence of two crestal areas, at the hanging wall and the footwall of fault F-100 (Fig. 4), should force gas to migrate vertically to two separate crests and result into two groups of stacked anomalies, not just one, as observed. This model seems then implausible; the alternative model is that the conduit belongs mainly to fault F-100 and its damage zone volume and that the individual anomalies composing the VAC are formed by injection of gas from this fault into the intervening host formations (Fig. 13D).

5.3. Mechanism of migration

Migration of hydrocarbons along faults is a challenging problem that have been extensively studied for several decades (Allan, 1989; Aydin, 2000; Smith, 1966). Faults are complex conduits that can activate and

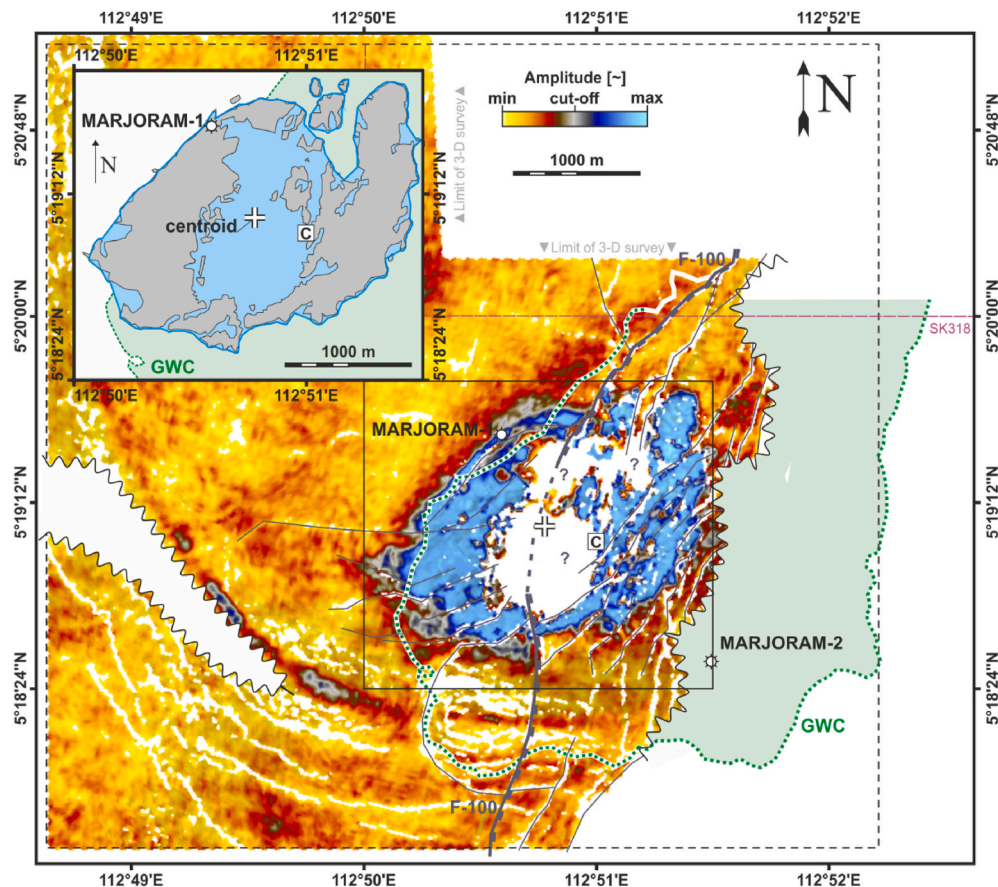


Fig. 10. Amplitude map of anomaly AA-500 with centroid (+), tentative interpretation of the fault network, position of the crest of the reservoir (C), location of the boreholes Marjoram-1 and Marjoram-2 and inset with amplitude margin extraction. The anomaly AA-500 is transected by fault F-100 with an apparent sinistral transcurrent motion of about 200 m. Note that the centroid of anomaly AA-500 is located nearly at the intersection with the fault plane.

allow fluids to migrate along them (e.g., [Sibson, 1982](#)) and constitute one of the most important seal by-pass systems for fluid migration across seals ([Cartwright et al., 2007](#)). Even during inactive periods faults may retain a permeability structure, that under specific boundary conditions can allow fluid migration ([Caine et al., 1996](#)).

Because the fault network above the Marjoram Gas Field is no longer active ([Fig. 2B](#)) it is excluded that gas migration, and the formation of this large VAC, occurred during fault slip. Therefore, we suggest that fault F-100, and its damage zone, could have been dilated because of large capillary pressure (e.g., [Cox, 1995](#); [Grauls et al., 1994](#)). Looking at the reconstructed pressure profile previously presented, the pressure exerted by the long gas column of the Marjoram Gas Field matches the fracture closing pressure of the overburden ([Fig. 4](#), pressure plots). This evidence, as previously anticipated, not only suggests that gas overpressure could have dilated fault F-100 allowing fluids to leak but could also justify that fault F-100 acted as the dominant conduit responsible for all the necessary stages of vertical gas migration to the top of the VAC ([Fig. 13D](#)).

The emplacement of the large gas cloud, that would then have started from high capillary pressure at the base of the fault (top reservoir), would have then proceeded sequentially, from the base to the top of the VAC. For each intervening host formation, the injection of gas at the observed injection points would have drain water radially emplacing the documented subcircular gas anomalies ([Fig. 13D](#)). The migration

process occurring in the overburden ([Fig. 3](#)), given the large gas column in the reservoir ([Fig. 4](#), pressure plots), could be still ongoing at present.

5.4. Implications

The specific distribution of the injection points of the analysed VAC above the Marjoram Gas Field highlights that the migration of free-phase gas along fault F-100 may not occur along a large volume of the fault damage zone ([Ligtenberg, 2005](#)), but instead it seems more likely restricted to a quite narrow corridor, spanning horizontally a few hundred meters ([Fig. 13B](#)). This mode of leakage is similar to the mechanism invoked by [Foschi et al. \(2018\)](#), and in line with works of [Rubino et al. \(2011\)](#), where the charge of stacked reservoir-like intervals occurs specifically along a central conduit region of focussed fluid flow rather spread along the entire extent of the gas-charged reservoir.

Another important point is that migration of gas along fault is often expected to proceed along the maximum dip of the fault where the buoyancy forces point along the direction of maximum pressure gradient between the overpressure region (e.g., the top reservoir) and the sea surface. Nevertheless, the direction of flow here observed diverges from a pure parallel direction of flow along the maximum dip of fault F-100 ([Figs. 10 and 13B](#)). This migration direction suggests that a preferential permeability pathway, which is likely to be formed once the fault open under excess pressure (mode I, e.g., [Gudmundsson, 2011](#)), represent the

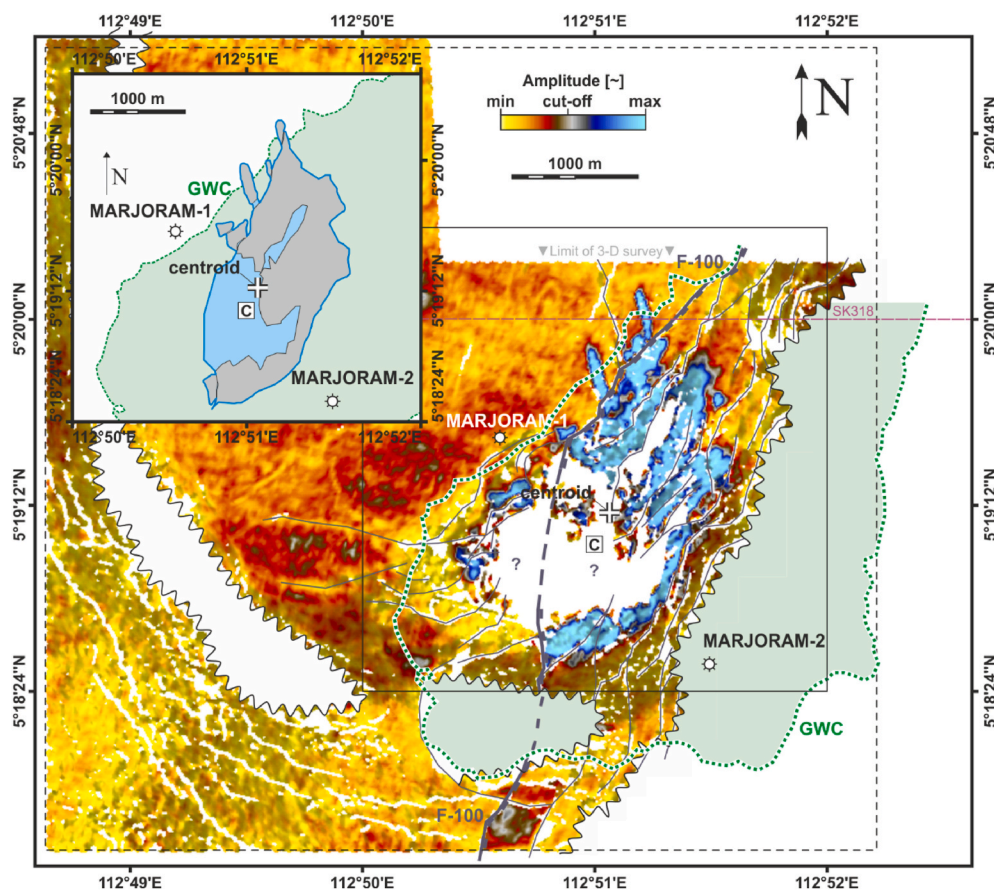


Fig. 11. Amplitude map of anomaly AA-450 with centroid (+), tentative interpretation of the fault network, position of the crest of the reservoir (C), location of the boreholes Marjoram-1 and Marjoram-2 and inset with amplitude margin extraction. The anomaly AA-450 is mostly bounded by fault F-100 and exhibits an irregular shape. Minor anomalies in the footwall of fault F-100 are not attributable to the emplacement of the main anomaly. The centroid of anomaly AA-450 is not interpreted as the injection point.

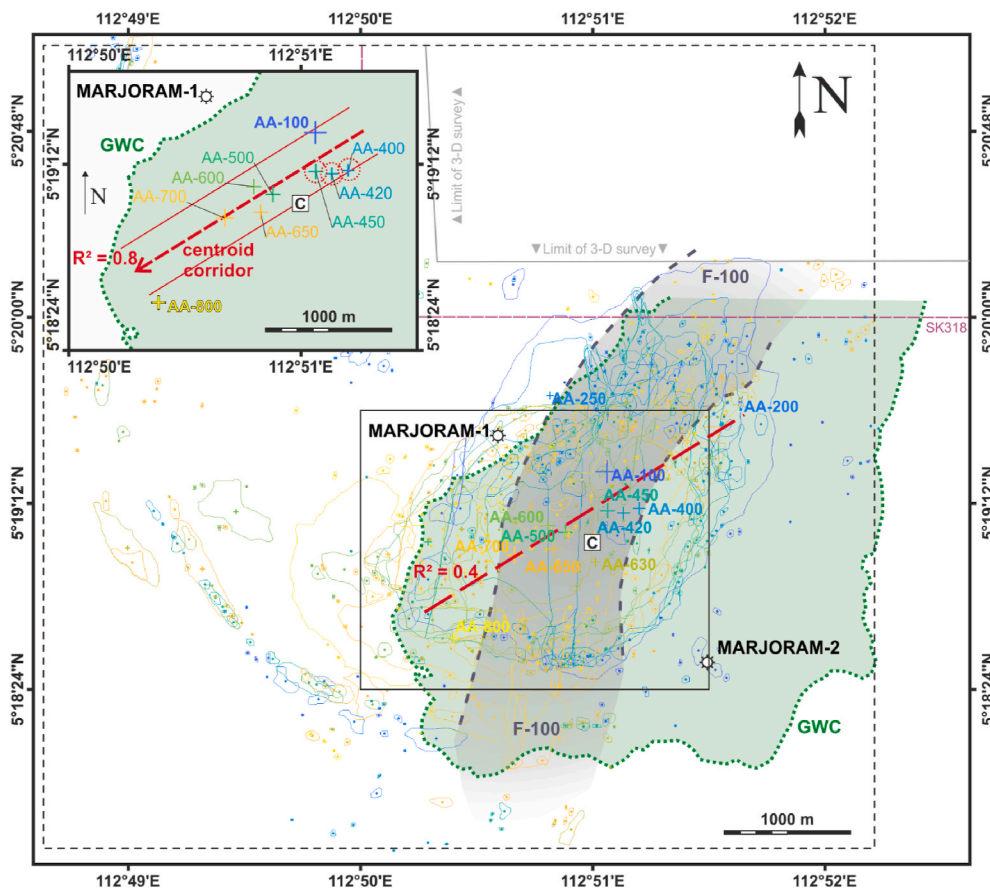


Fig. 12. Map showing the gas water contact (GWC) of the Marjoram Gas Field, fault F-100 from the Top of Carbonate to the top of the gas cloud, the position of the crest of the reservoir (C), the position of boreholes Marjoram-1 and Marjoram-2, the margins of the anomalies interpreted across 12 horizons within the overburden, and their centroids. The centroid symbol size (+) is scaled with respect to the area of the belonging anomaly and normalized against the size of AA-100 (the largest anomaly). Only the largest centroid for each map is labelled. The centroids, interpreted as injection points are aligned along a linear NE-SW oriented trend (red dashed arrow). Inset: centroid and centroid corridor, with position of the GWC and crest of the Marjoram Gas Field; the position of centroids of anomalies AA-400, AA-420 and AA-450 (red dashed circles) will be discussed in the Discussion. (For interpretation of the references to colour in this figure legend, the reader is referred to the Web version of this article.)

most efficient mechanism to release hydrocarbons from the Marjoram Gas Field.

The restricted, and “diagonal” pathway reconstructed in this study using the centroid analysis requires certainly further analysis (e.g., fault F-100, Fig. 3B). It is also true that the mechanism here invoked may well represent the dominant migration process rather than the full one – it is indeed expected that a proportion of gas escaping the Marjoram Gas Field could be driven along more pathways and may include a certain component of migration by capillary invasion in the sealing units (Jain and Juanes, 2009) and even a component of migration of gas in solution (Bjorkum et al., 1998). Nevertheless, the results point dominantly to a single migration mechanism, focused into a single migration pathway.

The implications from this work apply directly to those topseal-related tasks required for production and decommissioning from leaky hydrocarbon fields. The use of seismic data (Cartwright and Huuse, 2005), and detailed analysis, such as the one presented in this study, should provide more information on where hydrocarbon escape from topseals and specifically where the weakest part of the seal is with respect to the extent of the reservoir (Foschi and Cartwright, 2020). From a monitoring perspective analysis of this type should be routinely used, and updated on repeated seismic campaigns, to spot changes that could indicate a variation of the dominant mechanism of gas migration (escape) from the monitored site (e.g., CCS sites; Arts et al., 2004).

6. Conclusions

The main conclusions are as follows:

1. The Marjoram Gas Field is a multi-TCF gas field obscured by a large gas chimney composed of 10s of amplitude anomalies and consistent with the definition of vertical anomaly cluster
2. Detailed analysis of the vertical anomaly cluster, using centroid analysis, reveals a precise pathway for gas leakage across the overburden
3. Integration of the geophysical observations with pressure test data shows that mode I dilation of a fracture induced by the 455 m gas column in the reservoir is responsible for leakage

Authorship contribution

M.F. developed the study, interpreted, and integrated the geophysical data, wrote the manuscript. P.V.R. contributed to the development of the study and to the writing of the paper.

Declaration of competing interest

The authors declare that they have no known competing financial interests or personal relationships that could have appeared to influence the work reported in this paper.

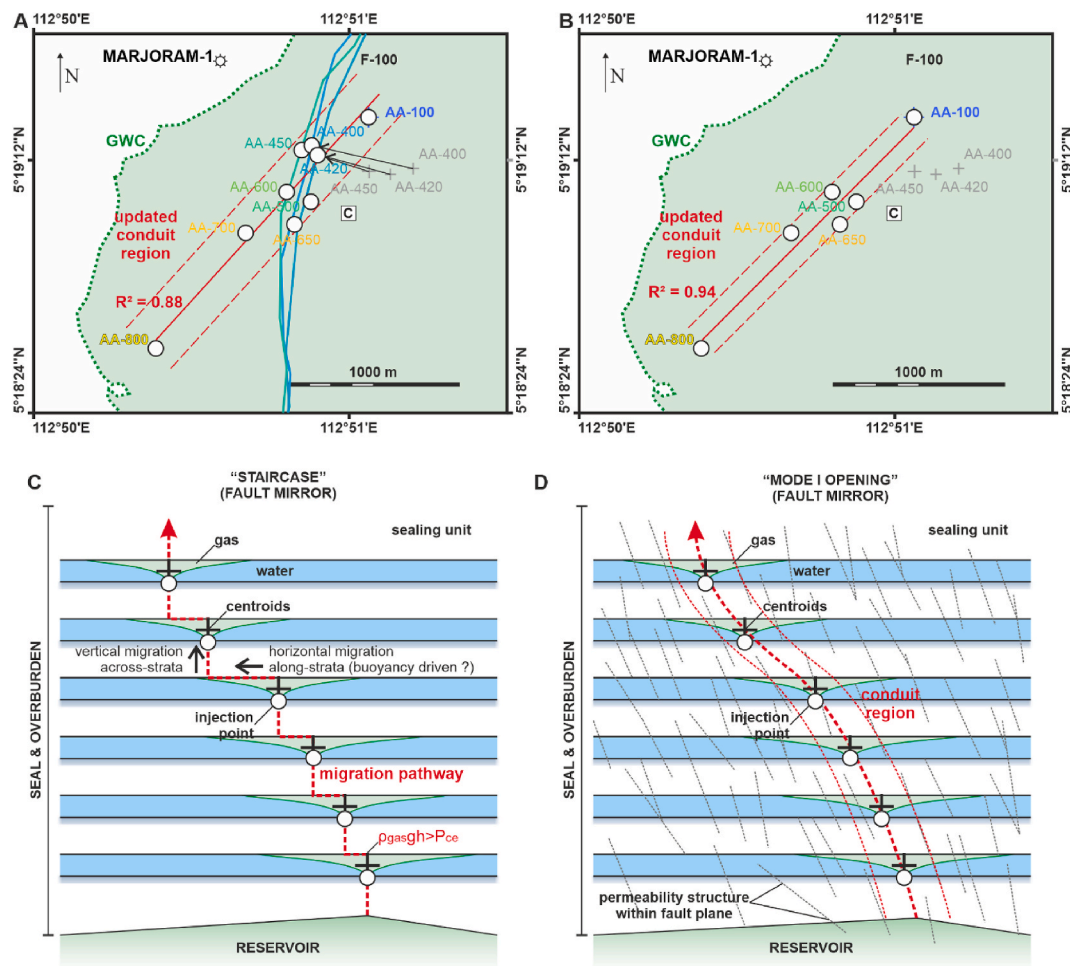


Fig. 13. Injection points and conduit region, with position of the GWC and crest of the Marjoram Gas Field. The injection points in A have been updated assuming fault F-100 as dominant conduit (see text). The updated injection points for anomalies AA-400, AA-430, and AA-450 results in a narrower and better-defined conduit region ($R^2 = 0.88$) (A). Removing the injection points of AA-400, AA-430, and AA-450 (see text), results into a narrower conduit region characterized by a higher correlation (B). Simplified cartoons showing the two scenarios discussed for gas migration across the seal and overburden above the Marjoram Gas Field. The scenarios are here based on a fixed distribution of injection points. In the staircase model (C) gas migrates vertically, by capillary invasion or hydraulic fracturing, and horizontally up-dip along the host permeable media. The resulting migration pathway can be simplified then as a “staircase” pattern where the fault does not necessarily influence the position of the vertical migration. Mode I fault opening model (D) assumes gas migration controlled by a pre-existing permeability structure produced, or enhanced, by the high gas pressure present at the base of the conduit (reservoir) (D).

Acknowledgments

We thank Shell Global Solutions International BV for sponsoring this project (FLUXUS) at University of Oxford. We are very thankful with Sarawak Shell Berhad and Petronas for academic access to seismic and well data and Belinda Ng for making it happen. We are grateful to Schlumberger and The Mathworks for providing software support. We thank Bruce Levell, Benedict Campbell, Charlie Lee, Murat Kilic, Flora Thiam, Cindy Chong, and Claudia Bertoni for their constructive comments. We also thank Hannu Seebeck, and one anonymous reviewer, for their insightful comments about the centroid method and its applicability, and for helping to improve this manuscript.

References

- Allan, U.S., 1989. Model for hydrocarbon migration and entrapment within faulted structures. *AAPG Bull.* 73 (7), 803–811.
- Andresen, K.J., Huuse, M., Schødt, N.H., Clausen, L.F., Seidler, L., 2011. Hydrocarbon plumbing systems of salt minibasins offshore Angola revealed by three-dimensional seismic analysis. *AAPG Bull.* 95 (6), 1039–1065.
- Arntsen, B., Wensaas, L., Løseth, H., Hermanrud, C., 2007. Seismic modeling of gas chimneys. *Geophysics* 72 (5), SM251–SM259.
- Arts, R., Eiken, O., Chadwick, A., Zweigel, P., van der Meer, B., Kirby, G., 2004. Seismic monitoring at the Sleipner underground CO₂ storage site (North Sea). *Geol. Soc. Lond. Sp. Publ.* 233 (1), 181–191.
- Aydin, A., 2000. Fractures, faults, and hydrocarbon entrapment, migration and flow. *Mar. Petrol. Geol.* 17 (7), 797–814.
- Bello, A., Heggland, R., Peacock, D.C.P., 2017. Pressure significance of gas chimneys. *Mar. Petrol. Geol.* 86, 402–407.
- Berg, R.R., 1975. Capillary pressures in stratigraphic traps. *AAPG Bull.* 59 (6), 939–956.
- Bertoni, C., Cartwright, J., Foschi, M., Martin, J., 2018. Spectrum of gas migration phenomena across multilayered sealing sequences. *AAPG (Am. Assoc. Pet. Geol.) Bull.* 102 (6), 1011–1034.
- Bjorkum, P.A., Walderhaug, O., Nadeau, P.H., 1998. Physical constraints on hydrocarbon leakage and trapping revisited. *Petrol. Geosci.* 4 (3), 237–239.
- Caine, J.S., Evans, J.P., Forster, C.B., 1996. Fault zone architecture and permeability structure. *Geology* 24 (11), 1025–1028.
- Cartwright, J., Huuse, M., 2005. 3D seismic technology: the geological ‘Hubble’. *Basin Res.* 17 (1), 1–20.
- Cartwright, J., Huuse, M., Aplin, A., 2007. Seal bypass systems. *AAPG Bull.* 91 (8), 1141–1166.
- Cox, S.F., 1995. Faulting processes at high fluid pressures: an example of fault valve behavior from the Wattle Gully Fault, Victoria, Australia. *J. Geophys. Res. Solid Earth* 100 (B7), 12841–12859.
- Domenico, S.N., 1974. Effect of water saturation on seismic reflectivity of sand reservoirs encased in shale. *Geophysics* 39 (6), 759–769.
- Doust, H., 1981. *Geology and Exploration History of Offshore Central Sarawak*.
- Epting, M., 1980. *Sedimentology of Miocene Carbonate Buildups, Central Luconia, Offshore Sarawak*. *Geol. Soc. Malaysia, Bulletin*, pp. 17–30.

- Foschi, M., Cartwright, J.A., 2016. South Malvinas/Falkland Basin: hydrocarbon migration and petroleum system. *Mar. Petrol. Geol.* 77, 124–140.
- Foschi, M., Cartwright, J.A., 2020. Seal failure assessment of a major gas field via integration of seal properties and leakage phenomena. *AAPG (Am. Assoc. Pet. Geol.) Bull.* 104 (8), 1627–1648.
- Foschi, M., Cartwright, J.A., Peel, F.J., 2014. Vertical anomaly clusters: evidence for vertical gas migration across multilayered sealing sequences. *AAPG (Am. Assoc. Pet. Geol.) Bull.* 98 (9), 1859–1884.
- Foschi, M., Cartwright, J.A., MacMinn, C.W., 2018. Sequential vertical gas charge into multilayered sequences controlled by central conduits. *AAPG (Am. Assoc. Pet. Geol.) Bull.* 102 (5), 855–883.
- Granli, J.R., Arntsen, B., Sollid, A., Hilde, E., 1999. Imaging through gas-filled sediments using marine shear-wave data. *Geophysics* 64 (3), 668–677.
- Graul, D.J., Baleix, J.M., 1994. Role of overpressures and in situ stresses in fault-controlled hydrocarbon migration: a case study. *Mar. Petrol. Geol.* 11 (6), 734–742.
- Gudmundsson, A., 2011. *Rock Fractures in Geological Processes*. Cambridge University Press.
- Heggland, R., 1997. Detection of gas migration from a deep source by the use of exploration 3D seismic data. *Mar. Geol.* 137 (1–2), 41–47.
- Heggland, R., 1998. Gas seepage as an indicator of deeper prospective reservoirs. A study based on exploration 3D seismic data. *Mar. Petrol. Geol.* 15 (1), 1–9.
- Heggland, R., 2005. Using Gas Chimneys in Seal Integrity Analysis: A Discussion Based on Case Histories.
- Heggland, R., 2013. Hydrocarbon trap classification based on associated gas chimneys. In: *Hydrocarbon Seepage: from Source to Surface*. Society of Exploration Geophysicists and American Association of Petroleum Geologists, pp. 221–230.
- Jain, A.K., Juanes, R., 2009. Preferential mode of gas invasion in sediments: grain-scale mechanistic model of coupled multiphase fluid flow and sediment mechanics. *J. Geophys. Res. Solid Earth* 114 (B8).
- Janjubah, H.T., Alansari, A., Ghosh, D.P., Bashir, Y., 2018. New approach towards the classification of microporosity in Miocene carbonate rocks, Central Luconia, offshore Sarawak, Malaysia. *J. Nat. Gas Geosci.* 3 (3), 119–133.
- Judd, A.G., Hovland, M., 1992. The evidence of shallow gas in marine sediments. *Contin. Shelf Res.* 12 (10), 1081–1095.
- King, R.C., Tingay, M.R., Hillis, R.R., Morley, C.K., Clark, J., 2010. Present-day stress orientations and tectonic provinces of the NW Borneo collisional margin. *J. Geophys. Res. Solid Earth* 115 (B10).
- Koša, E., 2015. Sea-level changes, shoreline journeys, and the seismic stratigraphy of Central Luconia, Miocene-present, offshore Sarawak, NW Borneo. *Mar. Petrol. Geol.* 59, 35–55.
- Lau, S., Huong, N., Nicolas, A., Shang-Yi, Y., Janssen, P., Winfield, P., 2014. MARJORAM-1 End of Well Report EXP.R.70993. Sarawak Shell Berhad.
- Ligtenberg, J.H., 2005. Detection of fluid migration pathways in seismic data: implications for fault seal analysis. *Basin Res.* 17 (1), 141–153.
- Løseth, H., Wensaas, L., Arntsen, B., 2002. April. Gas chimneys—indicating fractured cap rocks. In: *Extended Abstract Presented at the AAPG Hedberg Conference 'Near Surface Hydrocarbon Migration*, pp. 7–10.
- Løseth, H., Gading, M., Wensaas, L., 2009. Hydrocarbon leakage interpreted on seismic data. *Mar. Petrol. Geol.* 26 (7), 1304–1319.
- Lunt, P., Madon, M., 2017. *A Review of the Sarawak Cycles: History and Modern Application*.
- Mathieu, C., 2015. exploration well failures from the moray firth & central North Sea (UK). UK oil and gas authority. In: *21st Century Exploration Road Map Project*.
- Mehta, J., Bhaskaran, S., Row, Z., MacKinlay, W., Shaik, M.R., Rahim, M.H.A., Ngu, C.K., Kamaruzaman, M.A., Zainuddin, M.J., Mahmud, N., McKinney, D., Singh, N., Warrlich, G., 2016. MARJORAM-2 Appraisal Well Drilling and Subsurface EOWR, Document No: EP201603237279. Shell Malaysia Exploration and Production.
- Munns, J.W., 1985. The Valhall field: a geological overview. *Mar. Petrol. Geol.* 2 (1), 23–43.
- Myers, K., Rouillard, P., Zanella, E., 2019. *Exploration Performance in the UK and Norwegian North Sea*, vol. 494. Geological Society, London, Special Publications, pp. SP494–2018.
- Rankey, E.C., Schlaich, M., Mokhtar, S., Ghon, G., Ali, S.H., Poppelreiter, M., 2019. Seismic architecture of a Miocene isolated carbonate platform and associated off-platform strata (Central Luconia Province, offshore Malaysia). *Mar. Petrol. Geol.* 102, 477–495.
- Rubino, J.G., Velis, D.R., Sacchi, M.D., 2011. Numerical analysis of wave-induced fluid flow effects on seismic data: application to monitoring of CO₂ storage at the Sleipner field. *J. Geophys. Res. Solid Earth* 116 (B3).
- Rudolph, K.W., Goulding, F.J., 2017. Benchmarking exploration predictions and performance using 20+ yr of drilling results: one company's experience. *AAPG (Am. Assoc. Pet. Geol.) Bull.* 101 (2), 161–176.
- Sheriff, R.E., 1975. Factors affecting seismic amplitudes. *Geophys. Prospect.* 23 (1), 125–138.
- Sibson, R.H., 1982. Fault zone models, heat flow, and the depth distribution of earthquakes in the continental crust of the United States. *Bull. Seismol. Soc. Am.* 72 (1), 151–163.
- Smith, D.A., 1966. Theoretical considerations of sealing and non-sealing faults. *AAPG (Am. Assoc. Pet. Geol.) Bull.* 50 (2), 363–374.
- Smith, K.L., Steven, M.D., Jones, D.G., West, J.M., Coombs, P., Green, K.A., Barlow, T.S., Breward, N., Gwosdz, S., Krüger, M., Beaubien, S.E., 2013. Environmental Impacts of CO₂ Leakage: Recent Results from the ASGARD Facility, UK, vol. 37. *Energy Procedia*, pp. 791–799.
- Teige, G.M., Hermanrud, C., Thomas, W.H., Wilson, O.B., Bolås, H.M.N., 2005. Capillary resistance and trapping of hydrocarbons: a laboratory experiment. *Petrol. Geosci.* 11 (2), 125–129.
- Warner, M., Ratcliffe, A., Nangoo, T., Morgan, J., Umpleby, A., Shah, N., Vinje, V., Stekl, I., Guasch, L., Win, C., Conroy, G., 2013. Anisotropic 3D full-waveform inversion. *Geophysics* 78 (2), R59–R80.
- Widess, M.B., 1973. How thin is a thin bed? *Geophysics* 38 (6), 1176–1180.
- Zhao, B., MacMinn, C.W., Juanes, R., 2016. Wettability control on multiphase flow in patterned microfluidics. *Proc. Natl. Acad. Sci. Unit. States Am.* 113 (37), 10251–10256.